

## Research paper

# Synthesis, characterisation and electrochemistry of eight Fe coordination compounds containing substituted 2-(1-(4-R-phenyl-1H-1,2,3-triazol-4-yl)pyridine ligands, R = CH<sub>3</sub>, OCH<sub>3</sub>, COOH, F, Cl, CN, H and CF<sub>3</sub>

J. Conradie<sup>a,\*</sup>, M.M. Conradie<sup>a</sup>, Z. Mtshali<sup>a</sup>, D. van der Westhuizen<sup>a</sup>, K.M. Tawfiq<sup>b,c</sup>,  
M.J. Al-Jeboori<sup>c</sup>, S.J. Coles<sup>d</sup>, C. Wilson<sup>e</sup>, J.H. Potgieter<sup>b,f,\*</sup>

<sup>a</sup> Department of Chemistry, University of the Free State, P.O. Box 339, Bloemfontein 9300, South Africa

<sup>b</sup> Division of Chemistry and Environmental Science, Manchester Metropolitan University, Manchester M1 5GD, UK

<sup>c</sup> Department of Chemistry, College of Education for Pure Science (Ibn Al-Haitham), University of Baghdad, Baghdad, Iraq

<sup>d</sup> EPSRC National Crystallography Service, Chemistry, University of Southampton, Southampton SO17 1BJ, England, UK

<sup>e</sup> School of Chemistry, University of Glasgow, Joseph Black Building, University Avenue, Glasgow G12 8QQ, Scotland

<sup>f</sup> School of Chemical and Metallurgical Engineering, University of the Witwatersrand, Private Bag X3, Wits, 2050, South Africa



## ARTICLE INFO

**Keywords:**  
(1,2,3-Triazol-4-yl)pyridine  
Redox potential  
Iron  
DFT

## ABSTRACT

Eight different Dichloro(bis{2-[1-(4-R-phenyl)-1H-1,2,3-triazol-4-yl-κN<sup>3</sup>]pyridine-κN})iron(II) compounds, **2–9**, have been synthesised and characterised, where group R = CH<sub>3</sub> (L<sup>2</sup>), OCH<sub>3</sub> (L<sup>3</sup>), COOH (L<sup>4</sup>), F (L<sup>5</sup>), Cl (L<sup>6</sup>), CN (L<sup>7</sup>), H (L<sup>8</sup>) and CF<sub>3</sub> (L<sup>9</sup>). The single crystal X-ray structure was determined for the L<sup>3</sup> which was complemented with Density Functional Theory calculations for all complexes. The structure exhibits a distorted octahedral geometry, with the two triazole ligands coordinated to the iron centre positioned in the equatorial plane and the two chloro atoms in the axial positions. The values of the Fe<sup>II/III</sup> redox couple, observed at ca. –0.3 V versus Fc/Fc<sup>+</sup> for complexes **2–9**, varied over a very small potential range of 0.05 V. The observation that the different R substituents have virtually no effect on the values of the Fe<sup>II/III</sup> redox couple for all eight complexes **2–9**, is explained by the character of the highest molecular orbitals of complexes **2–9**, which do not show any communication of electron density between the various ligands and the metal Fe. However, the HOMOs of the free ligands L<sup>2</sup> – L<sup>9</sup>, display extended π-character over the entire ligand, explaining the sensitivity of the <sup>1</sup>H NMR C–H-triazole peak, which is dependent on the electron donating/withdrawing power of the R substituent attached to the 2-[1-(4-R-phenyl)-1H-1,2,3-triazol-4-yl]pyridine ligands.

## 1. Introduction

This study makes use of cycloaddition as synthetic method, an important strategy for constructing stereochemically complex heterocyclic compounds, which is a vital area of organic chemistry. Asymmetric [1,2] cycloaddition reactions, via chiral catalysts complexed to various metals, have recently been developed as new methods for designing technology specific complex heterocyclic compounds. Different five-membered ring systems can be very effectively synthesised via cycloaddition, starting with 2-atom or 3-atom precursors [1,2]. There are a variety of cycloaddition methods, e.g. also including 1,3-dipolar cycloadditions, which are very efficient in synthesising medicinal molecules and complex natural products [3]. A 1,2,3-triazole structure contains three adjacent nitrogen atoms with three available substitution sites and is a basic aromatic heterocyclic compound [4]. 1,2,3-Triazole is a useful building block [5]

when constructing more complex chemical compounds for specific applications, e.g. for medical applications (antimicrobial) [6] or chemical industrial use [7]. In this work a series eight of 1,2,3-triazole chromophores [10] were synthesized through the copper(I)-catalysed azide alkyne cycloaddition (CuAAC) “click” reaction [8] and then coordinated to iron (II) to prepare a variety of eight iron complexes **2–9** (Fig. 1), with potential application as photo-sensitizers for potential use in DSSCs. The first row transition metal Fe was chosen due its general availability and cost effectiveness as alternative to ruthenium metal [9], which is currently popular in dye solar cell research. For future evaluation of the compounds to be used as dyes in DSSCs, a detailed knowledge of their structure and properties is essential. The properties and characterisation of the chromophore ligands and their iron complexes, schematically shown in Fig. 1, are presented and discussed, including the crystal structure for **3**, as well as computational chemistry and electrochemistry results.

\* Corresponding authors.

E-mail address: [conradj@ufs.ac.za](mailto:conradj@ufs.ac.za) (J. Conradie).

<https://doi.org/10.1016/j.ica.2018.09.056>

Received 9 May 2018; Received in revised form 4 September 2018; Accepted 20 September 2018

Available online 22 September 2018

0020-1693/ © 2018 Elsevier B.V. All rights reserved.

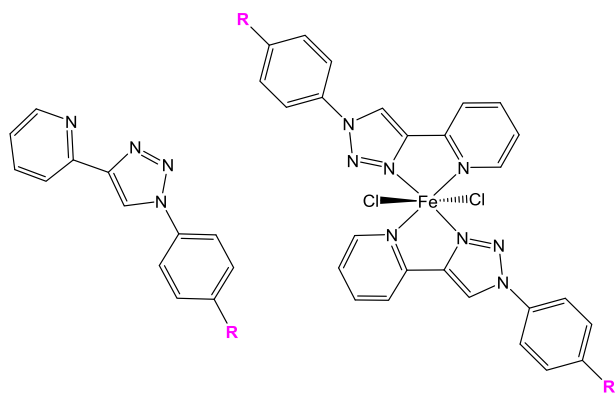


**Fig. 1.** Structure of the 1,2,3-triazole free ligands ( $L^2$ – $L^9$ ) and their respective iron complexes (**2**–**9**), where substituent R =  $\text{CH}_3$  ( $L^2$ ) [20],  $\text{OCH}_3$  ( $L^3$ ),  $\text{COOH}$  ( $L^4$ ), F ( $L^5$ ), Cl ( $L^6$ ), CN ( $L^7$ ), H ( $L^8$ ) and  $\text{CF}_3$  ( $L^9$ ).

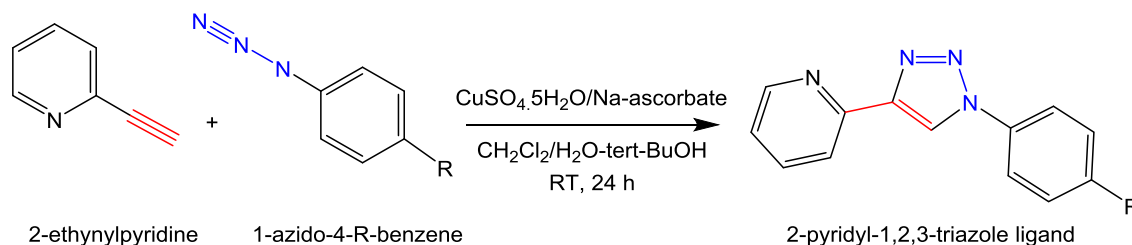
## 2. Methods and materials

### 2.1. Synthesis of (1,2,3-triazol-4-yl)pyridine ligands

The (1,2,3-triazol-4-yl)pyridine free ligands ( $L^2$  –  $L^9$ ) were synthesised and characterised, as has been described previously for  $L^2$  –  $L^9$  [10],  $L^2$  [11],  $L^3$  [12–14],  $L^6$  [15],  $L^8$  [16–18], see the reaction scheme in Scheme 1.

### 2.2. Synthesis of (1,2,3-triazol-4-yl)pyridine ligand iron(II) complexes

The general approach for the synthesis of all the iron(II) complexes was carried out according to a standard literature procedure, with small modifications as required [17]. For iron(II) complexes **2**, **3**, **5**–**9**, an appropriate amount of ferrous chloride (1 equiv. ca 3 mmol) was dissolved in methanol (10 ml) and added dropwise to a solution of the ligand (2 equiv. ca 6 mmol) in  $\text{CH}_2\text{Cl}_2$  (10 ml). The mixture was stirred at room temperature (RT) for 8–10 h, the solvent was removed under vacuum, the solid mass recovered and washed with several volumes of cold methanol and diethyl ether. Due to the poor solubility of the carboxylic group containing ligand  $L^4$ , the synthesis was changed as follow for complex **4**: ferrous chloride (1 equiv. ca 3 mmol) was dissolved in methanol (10 ml) and added dropwise to a solution of the ligand (2 equiv. ca 6 mmol) in DMSO (10 ml). The reaction mixture was stirred at RT for 10 min and then allowed to reflux for 24 h. The solvent was reduced in volume by a half under vacuum distillation and crushed ice was added to the solution. The precipitate was filtered before being washed twice with cold methanol and then diethyl ether. A similar poor solubility was reported for ligand btp, which is 2,6-bis(1-(4-(carboxy)benzyl)-1,2,3-triazol-4-yl)pyridine [19]. These methods proved very satisfactory and provided good yields, ranging from 73 to 83% (see below for exact yields). The reaction for **2**, **3**, **5**–**9** is represented in Scheme 2. The characterisation data of the paramagnetic Fe(II) complexes are given below.



**Scheme 1.** Preparation route for the 2-pyridyl-1,2,3-triazole free ligands ( $L^2$ – $L^9$ ) from an azide and alkyne by the Cu(I) catalyzed “click” reaction where substituent R =  $\text{CH}_3$  ( $L^2$ ),  $\text{OCH}_3$  ( $L^3$ ),  $\text{COOH}$  ( $L^4$ ), F ( $L^5$ ), Cl ( $L^6$ ), CN ( $L^7$ ), H ( $L^8$ ) and  $\text{CF}_3$  ( $L^9$ ).

#### 2.2.1. Characterisation of dichloro(bis{2-[1-(4-methylphenyl)-1H-1,2,3-triazol-4-yl- $\kappa\text{N}^3$ ]pyridine- $\kappa\text{N}$ })iron(II), complex **2** (containing $L^2$ with R = $\text{CH}_3$ ) [20]

Yield 83%, mp. 308–310 °C. IR:  $\bar{\nu}$  ( $\text{cm}^{-1}$ ): 3063, 3047, 3025, 1605, 1595, 1571, 1522, 1473, 1448, 1267, 1258, 1063, 1054, 1015, 1004, 886, 815, 786, 553. UV–Vis (DMSO)  $\lambda_{\text{max}}$ : The Fe(II) complex showed absorption bands at 259 nm,  $\epsilon_{\text{max}} = 65\,500 \text{ dm}^3 \text{ mol}^{-1} \text{ cm}^{-1}$ , 287 nm,  $\epsilon_{\text{max}} = 52\,000 \text{ dm}^3 \text{ mol}^{-1} \text{ cm}^{-1}$ , 326 nm,  $\epsilon_{\text{max}} = 4783 \text{ dm}^3 \text{ mol}^{-1} \text{ cm}^{-1}$ , 908 nm,  $\epsilon_{\text{max}} = 85 \text{ dm}^3 \text{ mol}^{-1} \text{ cm}^{-1}$ . HRMS TOF (ESI+) (water: acetonitrile = 1:3) with the highest molecular weight ion peak matching, was observed at  $m/z = 563.1135$  (80%) and is attributed to  $[\text{Fe}(L^2)_2\text{Cl}_2] - \text{Cl}]^+$ . The calculated value for  $[(\text{C}_{28}\text{H}_{24}\text{N}_8\text{FeCl})]^+$  is 563.1162.  $\mu_{\text{eff}} = 5.26 \text{ B.M.}$  Elemental Anal. Calc. for  $\text{C}_{28}\text{H}_{24}\text{N}_8\text{Cl}_2\text{Fe}$ : C, 56.1; H, 4.0; N 18.7. Found: C, 56.0; H, 4.1; N 18.8%.

#### 2.2.2. Characterisation of dichloro(bis{2-[1-(4-methoxyphenyl)-1H-1,2,3-triazol-4-yl- $\kappa\text{N}^3$ ]pyridine- $\kappa\text{N}$ })iron(II), complex **3** (containing $L^3$ with R = $\text{OCH}_3$ )

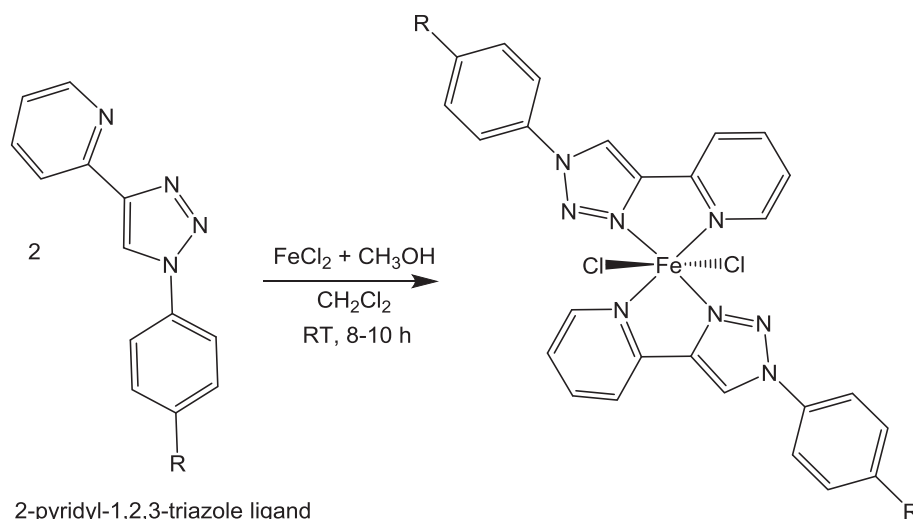
Yield 83%, mp. 308–310 °C. IR:  $\bar{\nu}$  ( $\text{cm}^{-1}$ ): 3054, 3032, 3012, 2965, 2865, 2838, 1606, 1571, 1518, 1469, 1448, 1289, 1261, 1182, 1065, 1055, 1017, 1002, 979, 858, 825, 786, 719. UV–Vis (DMSO)  $\lambda_{\text{max}}$ : The Fe(II) complex showed absorption bands at 256 nm,  $\epsilon_{\text{max}} = 35\,500 \text{ dm}^3 \text{ mol}^{-1} \text{ cm}^{-1}$ , 291 nm,  $\epsilon_{\text{max}} = 17\,500 \text{ dm}^3 \text{ mol}^{-1} \text{ cm}^{-1}$ , 333 nm,  $\epsilon_{\text{max}} = 3810 \text{ dm}^3 \text{ mol}^{-1} \text{ cm}^{-1}$ , 922 nm,  $\epsilon_{\text{max}} = 65 \text{ dm}^3 \text{ mol}^{-1} \text{ cm}^{-1}$ . HRMS TOF (ESI+) (water: acetonitrile = 1:3) with the highest molecular weight ion peak matching, was observed at  $m/z = 595.1055$  (88%) and is attributed to  $[\text{Fe}(L^3)_2\text{Cl}_2] - \text{Cl}]^+$ . The calculated value for  $[(\text{C}_{28}\text{H}_{24}\text{ClFeN}_8\text{O}_2)]^+$  is 595.1060.  $\mu_{\text{eff}} = 5.07 \text{ B.M.}$  Elemental Anal. Calc. for  $\text{C}_{28}\text{H}_{24}\text{N}_8\text{Cl}_2\text{O}_2\text{Fe}$ : C, 53.3; H, 3.8; N 17.8. Found: C, 53.0; H, 3.71; N 17.5%.

#### 2.2.3. Characterisation of dichloro(bis{4-[4-(pyridin-2-yl- $\kappa\text{N}$ )-1H-1,2,3-triazol-1-yl- $\kappa\text{N}^3$ ]benzoic acid})iron(II), complex **4** (containing $L^4$ with R = $\text{COOH}$ )

Yield 73%, mp. 348–350 °C. IR:  $\bar{\nu}$  ( $\text{cm}^{-1}$ ): 3085, 1724, 1604, 1589, 1514, 1471, 1450, 1406, 1372, 1254, 1173, 1104, 1055, 1018, 1004, 978, 857, 774. UV–Vis (DMSO)  $\lambda_{\text{max}}$ : The Fe(II) complex showed absorption bands at 258 nm,  $\epsilon_{\text{max}} = 181\,600 \text{ dm}^3 \text{ mol}^{-1} \text{ cm}^{-1}$ , 291 nm,  $\epsilon_{\text{max}} = 86\,500 \text{ dm}^3 \text{ mol}^{-1} \text{ cm}^{-1}$ , 332 nm,  $\epsilon_{\text{max}} = 7053 \text{ dm}^3 \text{ mol}^{-1} \text{ cm}^{-1}$ . HRMS TOF (MALDI) with the highest molecular weight ion peak matching, was observed at  $m/z = 623.1$  (100%) and is related to  $[\text{Fe}(L^4)_2\text{Cl}_2] - \text{Cl}]^+$ . The calculated value for  $[\text{C}_{28}\text{H}_{20}\text{N}_8\text{FeO}_4\text{Cl}]^+$  is 623.100.  $\mu_{\text{eff}} = 5.1 \text{ B.M.}$  Elemental Anal. Calc. for  $\text{C}_{28}\text{H}_{20}\text{N}_8\text{Cl}_2\text{O}_4\text{Fe}$ : C, 51.0; H, 3.1; N 17.0. Found: C, 51.3; H, 2.9; N 16.8%.

#### 2.2.4. Characterisation of dichloro(bis{2-[1-(4-fluorophenyl)-1H-1,2,3-triazol-4- $\kappa\text{N}^3$ ]pyridine- $\kappa\text{N}$ })iron(II), complex **5** (containing $L^5$ with R = F)

Yield 75%, mp. 258–260 °C. IR:  $\bar{\nu}$  ( $\text{cm}^{-1}$ ): 3065, 3041, 3026, 1605, 1578, 1515, 1472, 1453, 1412, 1333, 1239, 1258, 1159, 1061, 1015, 1005, 979, 837, 788, 718. UV–Vis (DMSO)  $\lambda_{\text{max}}$ : The Fe(II) complex showed absorption bands at 257 nm,  $\epsilon_{\text{max}} = 69\,630 \text{ dm}^3 \text{ mol}^{-1} \text{ cm}^{-1}$ , 286 nm,  $\epsilon_{\text{max}} = 3111 \text{ dm}^3 \text{ mol}^{-1} \text{ cm}^{-1}$ , 329 nm,  $\epsilon_{\text{max}} = 3380 \text{ dm}^3 \text{ mol}^{-1} \text{ cm}^{-1}$ . HRMS TOF (MALDI) with the highest molecular weight ion peak



**Scheme 2.** Synthesis of the various eight  $[\text{Fe}(\text{L}^n)_2\text{Cl}_2]$  complexes (where  $n = 2-9$ ) from the ligands,  $\text{L}_2 - \text{L}_9$ . Substituent  $\text{R} = \text{CH}_3$  ( $\text{L}^2$ ),  $\text{OCH}_3$  ( $\text{L}^3$ ),  $\text{COOH}$  ( $\text{L}^4$ ),  $\text{F}$  ( $\text{L}^5$ ),  $\text{Cl}$  ( $\text{L}^6$ ),  $\text{CN}$  ( $\text{L}^7$ ),  $\text{H}$  ( $\text{L}^8$ ) and  $\text{CF}_3$  ( $\text{L}^9$ ).

matching, was observed at  $m/z = 571.0635$  (35%) and is assigned to  $[\text{Fe}(\text{L}^5)_2\text{Cl}_2] - \text{Cl}]^+$ . The calculated value for  $[\text{C}_{26}\text{H}_{18}\text{F}_2\text{N}_8\text{FeCl}]^+$  is 571.0660.  $\mu_{\text{eff}} = 4.87\text{B.M.}$  Elemental Anal. Calc. for  $\text{C}_{26}\text{H}_{18}\text{N}_8\text{Cl}_2\text{F}_2\text{Fe}$ : C, 51.4; H, 3.0; N 18.5. Found: C, 51.6; H, 2.8; N 18.2%.

#### 2.2.5. Characterisation of dichloro[bis{2-[1-(4-chlorophenyl)-1H-1,2,3-triazol-4-yl- $\kappa\text{N}^3$ ]pyridine- $\kappa\text{N}$ }]iron(II), complex 6 (containing $\text{L}^6$ with $\text{R} = \text{Cl}$ )

Yield 79%, mp. 258–260 °C. IR:  $\bar{\nu}$  ( $\text{cm}^{-1}$ ): 3051, 3023, 3005, 1606, 1591, 1570, 1502, 1472, 1448, 1405, 1267, 1257, 1151, 1134, 1095, 1061, 1052, 1013, 1003, 977, 860, 825, 808, 789, 711. UV-Vis (DMSO)  $\lambda_{\text{max}}$ : The Fe(II) complex showed absorption bands at 258 nm,  $\epsilon_{\text{max}} = 58571 \text{ dm}^3 \text{ mol}^{-1} \text{ cm}^{-1}$ , 287 nm,  $\epsilon_{\text{max}} = 47143 \text{ dm}^3 \text{ mol}^{-1} \text{ cm}^{-1}$ , 332 nm,  $\epsilon_{\text{max}} = 4060 \text{ dm}^3 \text{ mol}^{-1} \text{ cm}^{-1}$ , 386 nm,  $\epsilon_{\text{max}} = 2020 \text{ dm}^3 \text{ mol}^{-1} \text{ cm}^{-1}$ . HRMS (ESI+) (water: acetonitrile = 1:3) with the highest molecular weight ion peak matching, was observed at  $m/z = 603.0050$  (75%) and is related to  $[\text{Fe}(\text{L}^6)_2\text{Cl}_2] - \text{Cl}]^+$ . The calculated value for  $[\text{C}_{26}\text{H}_{18}\text{N}_8\text{Cl}_4\text{Fe}]^+$  is 603.0069.  $\mu_{\text{eff}} = 5.10\text{B.M.}$  Elemental Anal. Calc. for  $\text{C}_{26}\text{H}_{18}\text{N}_8\text{Cl}_4\text{Fe}$ : C, 48.8; H, 2.8; N 17.5. Found: C, 49.0; H, 3.0; N 17.3%.

#### 2.2.6. Characterisation of dichloro[bis{4-[4-(pyridin-2-yl- $\kappa\text{N}$ )-1H-1,2,3-triazol-1-yl- $\kappa\text{N}^3$ ]benzonitrile}]iron(II), complex 7 (containing $\text{L}^7$ with $\text{R} = \text{CN}$ )

Yield 83%, mp. 308–310 °C. IR:  $\bar{\nu}$  ( $\text{cm}^{-1}$ ): 3071, 3057, 3025, 3012, 2233, 1604, 1591, 1572, 1514, 1471, 1451, 1410, 1287, 1258, 1259, 1140, 1061, 1052, 1016, 1006, 977, 846, 787, 717. UV-Vis (DMSO)  $\lambda_{\text{max}}$ : The Fe(II) complex showed absorption bands at 256 nm,  $\epsilon_{\text{max}} = 138750 \text{ dm}^3 \text{ mol}^{-1} \text{ cm}^{-1}$ , 289 nm,  $\epsilon_{\text{max}} = 56250 \text{ dm}^3 \text{ mol}^{-1} \text{ cm}^{-1}$ , 950 nm,  $\epsilon_{\text{max}} = 45 \text{ dm}^3 \text{ mol}^{-1} \text{ cm}^{-1}$ . HRMS TOF (ESI+) (water: acetonitrile = 1:3) with the highest molecular weight ion peak matching, was observed at  $m/z = 585.0738$  (70%) and is assigned to  $[\text{Fe}(\text{L}^7)_2\text{Cl}_2] - \text{Cl}]^+$ . The calculated value for  $[\text{C}_{28}\text{H}_{18}\text{N}_{10}\text{ClFe}]^+$  is 585.0754.  $\mu_{\text{eff}} = 4.26\text{B.M.}$  Elemental Anal. Calc. for  $\text{C}_{28}\text{H}_{18}\text{N}_{10}\text{Cl}_2\text{Fe}$ : C, 54.1; H, 2.9; N 22.6. Found: C, 54.4; H, 3.1; N 22.6%.

#### 2.2.7. Characterisation of dichloro[bis{2-(1-phenyl-1H-1,2,3-triazol-4-yl- $\kappa\text{N}^3$ ]pyridine- $\kappa\text{N}$ }]iron(II), complex 8 (containing $\text{L}^8$ with $\text{R} = \text{H}$ )

Yield 81%, mp. 336–338 °C. IR:  $\bar{\nu}$  ( $\text{cm}^{-1}$ ): 3064, 3053, 3026, 3009, 1606, 1594, 1575, 1504, 1471, 1444, 1267, 1259, 1063, 1054, 1016, 1004, 977, 913, 861, 815, 785, 756, 725, 686. UV-Vis (DMSO)  $\lambda_{\text{max}}$ : The Fe(II) complex showed absorption bands at 258 nm,  $\epsilon_{\text{max}} = 62593 \text{ dm}^3 \text{ mol}^{-1} \text{ cm}^{-1}$ , 286 nm,  $\epsilon_{\text{max}} = 32963 \text{ dm}^3 \text{ mol}^{-1} \text{ cm}^{-1}$ , 333 nm,  $\epsilon_{\text{max}} = 52917 \text{ dm}^3 \text{ mol}^{-1} \text{ cm}^{-1}$ , 522 nm,  $\epsilon_{\text{max}} =$

$190 \text{ dm}^3 \text{ mol}^{-1} \text{ cm}^{-1}$ , 756 nm,  $\epsilon_{\text{max}} = 885 \text{ dm}^3 \text{ mol}^{-1} \text{ cm}^{-1}$ . HRMS TOF (ESI+) (water: acetonitrile = 1:3) with the highest molecular weight ion peak matching, was observed at  $m/z = 535.0835$  (60%) and is related to  $[\text{Fe}(\text{L}^8)_2\text{Cl}_2] - \text{Cl}]^+$ . The calculated value for  $[\text{C}_{26}\text{H}_{20}\text{N}_8\text{ClFe}]^+$  is 535.0849.  $\mu_{\text{eff}} = 4.66\text{B.M.}$  Elemental Anal. Calc. for  $\text{C}_{26}\text{H}_{20}\text{N}_8\text{Cl}_2\text{Fe}$ : C, 54.7; H, 3.5; N 19.6. Found: C, 54.5; H, 3.8; N 19.6%.

#### 2.2.8. Characterisation of dichloro[bis{2-[1-[4-(trifluoromethyl)phenyl]-1H-1,2,3-triazol-4-yl- $\kappa\text{N}^3$ ]pyridine- $\kappa\text{N}$ }]iron(II), complex 9 (containing $\text{L}^9$ with $\text{R} = \text{CF}_3$ )

Yield 83%, mp. 274–276 °C. IR:  $\bar{\nu}$  ( $\text{cm}^{-1}$ ): 3063, 3047, 3025, 1605, 1595, 1571, 1522, 1473, 1448, 1267, 1258, 1060, 1049, 1015, 1005, 886, 815, 786. UV-Vis (DMSO)  $\lambda_{\text{max}}$ : The Fe(II) complex showed absorption bands at 258 nm,  $\epsilon_{\text{max}} = 58947 \text{ dm}^3 \text{ mol}^{-1} \text{ cm}^{-1}$ , 288 nm,  $\epsilon_{\text{max}} = 48947 \text{ dm}^3 \text{ mol}^{-1} \text{ cm}^{-1}$ , 326 nm,  $\epsilon_{\text{max}} = 4511 \text{ dm}^3 \text{ mol}^{-1} \text{ cm}^{-1}$ , 566 nm,  $\epsilon_{\text{max}} = 461 \text{ dm}^3 \text{ mol}^{-1} \text{ cm}^{-1}$ , 590 nm,  $\epsilon_{\text{max}} = 453 \text{ dm}^3 \text{ mol}^{-1} \text{ cm}^{-1}$  respectively. HRMS TOF (MALDI) with the highest molecular weight ion peak matching, was observed at  $m/z = 671.1$  (100%) and is attributed to  $[\text{Fe}(\text{L}^9)_2\text{Cl}_2] - \text{Cl}]^+$ . The calculated value for  $[\text{C}_{28}\text{H}_{18}\text{ClF}_6\text{N}_8\text{Fe}]^+$  is 671.100.  $\mu_{\text{eff}} = 4.72\text{B.M.}$  Elemental Anal. Calc. for  $\text{C}_{28}\text{H}_{18}\text{N}_8\text{Cl}_2\text{F}_6\text{Fe}$ : C, 47.6; H, 2.6; N 15.9. Found: C, 47.7; H, 2.3; N 15.7%.

### 2.3. Instrumental conditions and measurement parameters

Infrared (ATR-FTIR IR) spectra were recorded using a smart diamond ATR attachment on a Thermo-Nicolet FT-IR Spectrometer (AVATAR 320), over a range of 4000–400  $\text{cm}^{-1}$ . Mass spectra were performed at EPSRC Mass Spectrometry Service Centre, University of Wales, Swansea and University of Sheffield. The instrument used was the 'WATERS LCT premier', the solvent was water/acetonitrile (1:3), while the ionisation was electrospray (ESI+ and ES-). Thermofisher LTQ Orbitrap XL, used to analyse volatile molecules in the mass range of  $m/z$  50–2000 or  $m/z$  200–4000 Daltons. UV-Vis spectra were obtained on a PerkinElmer Lambda 40 UV/Vis spectrometer. Each sample ( $1 \times 10^{-5} \text{ M}$ ) was analysed using a constant blank of acetonitrile. A pair of identical quartz cells with a path length of 1 cm were used to reduce the interference from the cells themselves. Further spectra was obtained for specific complexes at a concentration of  $1 \times 10^{-3} \text{ M}$  when some absorbance was visible albeit at a very low level. The absorbance was measured over a wavelength range of 250 nm–900 nm.

## 2.4. Magnetic susceptibility

Magnetic susceptibility of the complexes was measured with a Gouy magnetic susceptibility balance. The gram magnetic susceptibility for a substance is calculated from:

$$\chi_g = (C_{\text{bal}})l(R - R_0)/(10^9)(m)$$

where  $l$  = height of sample in the tube in units of centimeters,  $m$  = mass of the sample in units of grams,  $R$  = reading for tube plus sample,  $R_0$  = reading for the empty tube and  $C_{\text{bal}}$  = balance calibration constant = 1.0. The molar magnetic susceptibility is then calculated from the gram magnetic susceptibility using the following equation.

$$\chi_m = (\chi_g) (\text{molar mass})$$

The effective magnetic moment for a particular substance is calculated from the molar magnetic susceptibility [21] using the following equation ( $T$  represents the Kelvin temperature (294 K)):

$$\mu_{\text{eff}} = 2.83 [(\chi_m)(T)]^{1/2}$$

## 2.5. X-ray diffraction

The crystal of complex **3**  $[\text{Fe}(\text{L}^3)_2\text{Cl}_2]$  with ligand  $\text{L}^3$  (where  $R = \text{OCH}_3$ ) suitable for a single crystal diffraction data collection, was obtained by slow evaporation in a hot mixture of a DMSO:acetonitrile = 1:9 solution, under ambient conditions. Single crystal X-ray diffraction data were collected using a Rigaku Saturn 724 + area detector, mounted at the window of an FR-E + rotating anode generator, with wavelength Mo  $K\alpha$ ,  $\lambda = 0.71075 \text{ \AA}$  [22]. The crystals were mounted on a Mitegen loop and data was collected at 100 K, under nitrogen flow from an Oxford Cryosystems Cobra device. The structures were solved by direct methods, using the program SHELXS-97 within OLEX2 [23]. All refinements on  $F_o^2$  by full-matrix least squares refinement, were performed using the SHELXL-97 program package [24] within the OLEX2 software. All non-hydrogen atoms were refined with anisotropic atomic displacement parameters, and hydrogen atoms were added at calculated positions and included as part of a riding model with C–H (aromatic)  $0.95 \text{ \AA}$   $U_{\text{ISO}} = 1.2U_{\text{eq}}$  (C); and C–H (methyl)  $0.98 \text{ \AA}$   $U_{\text{ISO}} = 1.5U_{\text{eq}}$  (C) [57]. A perspective drawing of the molecular structure of complex  $[\text{Fe}(\text{L}^3)_2\text{Cl}_2]$ , showing the atom numbering scheme, is shown in Fig. 6. Crystallographic data is presented in Table 1, with selected bond lengths ( $\text{\AA}$ ) and bond angles ( $^\circ$ ) listed in Table 2. Additional crystallographic data are available free of charge from the Cambridge Crystallographic Data Centre (Deposition number CCDC 1585946).

## 2.6. Cyclic voltammetry

Cyclic voltammetry measurements [25] were performed on  $0.05 \text{ mmol dm}^{-3}$  or saturated compound solutions, in dry acetonitrile/DMSO solution (Aldrich, Biotech grade 99.93 + % purity, anhydrous, kept under purified argon), under a blanket of purified argon at  $25^\circ\text{C}$ , utilizing a BAS 100B/W electrochemical analyzer. Due to the poor solubility of the compound in acetonitrile, each of the eight complexes was first dissolved in 0.5 ml DMSO, after which 1.5 ml acetonitrile was added. The supporting electrolyte was  $0.1 \text{ mol dm}^{-3}$  tetra-*n*-butylammonium hexafluorophosphate, ( $^t\text{Bu}_4\text{N})(\text{PF}_6)$  (Fluka electrochemical grade). A three-electrode cell, with a glassy carbon (surface area  $7.07 \times 10^{-6} \text{ m}^2$ ) working electrode, Pt auxiliary electrode and a  $\text{Ag}/\text{Ag}^+$  ( $0.010 \text{ mol dm}^{-3}$   $\text{AgNO}_3$  in  $\text{CH}_3\text{CN}$ ) reference electrode [26], mounted on a Luggin capillary, was used [27,28]. All temperatures were kept constant, within  $0.5^\circ\text{C}$ . Successive experiments under the same experimental conditions showed that all reduction and formal reduction potentials were reproducible within 0.005 V. All cited potentials were referenced against the  $\text{Fc}/\text{Fc}^+$  couple, as suggested by

**Table 1**

Crystallographic data for complex  $[\text{Fe}(\text{L}^3)_2\text{Cl}_2]$  (with group  $R = \text{OCH}_3$  on ligand  $\text{L}^3$ ).

Empirical formula	$\text{C}_{28}\text{H}_{24}\text{Cl}_2\text{FeN}_8\text{O}_2$
$M_r$	631.30
Temp/K	100(2) K
Cryst. syst.	Monoclinic
Space group	$P2_1/c$
$a/\text{\AA}$	10.3599(7)
$b/\text{\AA}$	13.1029(8)
$c/\text{\AA}$	10.2300(6)
$\alpha/^\circ$	90.00
$\beta/^\circ$	96.161(7)
$\gamma/^\circ$	90.00
$V/\text{\AA}^3$	1380.65(15)
$Z$	2
$R_{\text{int}}$	0.0387
$D_{\text{calcd}}/\text{g cm}^{-3}$	1.519
Refln (all/ind/obsd)	6581/3143/2754
$\mu/\text{mm}^{-1}$	0.783
$R1$ (obsd data: $F^2 > 2\sigma(F^2)$ ) <sup>a</sup>	0.0398
w $R2$ (all data) <sup>a</sup>	0.1063

**Table 2**

Selected bond lengths ( $\text{\AA}$ ) and bond angles ( $^\circ$ ) for complex  $[\text{Fe}(\text{L}^3)_2\text{Cl}_2]$  (with  $R = \text{OCH}_3$ ).

Bond distance ( $\text{\AA}$ )	Bond angles ( $^\circ$ )		
C7–C11	1.375(3)	$\text{N}_{(\text{pyridine})} \text{1–Fe–N}_{(\text{pyridine})} \text{1}^i$	180
N8–N9	1.311(2)	$\text{N}_{(\text{triazole})} \text{1}^i \text{–Fe–N}_{(\text{triazole})} \text{1}$	180
N9–N10	1.354(2)	$\text{N}_{(\text{pyridine})} \text{1–Fe–N}_{(\text{triazole})} \text{1}^i$	104.10(6)
N8–C7	1.360(2)	$\text{N}_{(\text{pyridine})} \text{1–Fe–N}_{(\text{triazole})} \text{1}$	75.90(6)
$\text{Fe–N}_{(\text{pyridine})} \text{1}$	2.2018(15)	$\text{N}_{(\text{pyridine})} \text{1–Fe–Cl 1}$	89.80(4)
$\text{Fe–N}_{(\text{triazole})} \text{1}$	2.1838(16)	$\text{N}_{(\text{pyridine})} \text{1}^i \text{–Fe–Cl 1}$	90.20(4)
$\text{Fe–Cl 1}$	2.4456(5)	$\text{N}_{(\text{triazole})} \text{1}^i \text{–Fe–Cl 1}$	90.20(4)
		$\text{N}_{(\text{triazole})} \text{1–Fe–Cl 1}$	89.80(4)
		$\text{Cl 1}^i \text{–Fe–Cl 1}$	180

<sup>i</sup> Symmetry transformation used to generate equivalent atoms  $-x + 1, -y + 1, -z$ .

IUPAC [29]. Ferrocene exhibited a formal reduction potential of  $E^{\circ'} = 0.090 \text{ V}$  vs.  $\text{Ag}/\text{Ag}^+$ , a peak separation of  $\Delta E_p = E_{\text{pa}} - E_{\text{pc}} = 0.070 \text{ V}$ , as well as a ratio  $i_{\text{pc}}/i_{\text{pa}} = 0.99$  under our experimental conditions.  $E_{\text{pa}}$  ( $E_{\text{pc}}$ ) = anodic (cathodic) peak potential, and  $i_{\text{pa}}$  ( $i_{\text{pc}}$ ) = anodic (cathodic) peak current.  $E^{\circ'}$  ( $\text{Fc}/\text{Fc}^+$ ) = 0.400 V vs. NHE [30], and SCE = 0.244 V vs. NHE.

## 2.7. Theoretical approach

Density functional theory (DFT) calculations were performed via the B3LYP functional, as implemented in the Gaussian 09 package [31], using the triple- $\zeta$  basis set 6-311G(d,p). The ligands  $\text{L}^2 - \text{L}^8$ , as well as the complex  $[\text{Fe}(\text{L}^8)_2\text{Cl}_2]$ , with  $R = \text{H}$  on ligand  $\text{L}^8$ , were optimized. The possible spin states of  $[\text{Fe}(\text{L}^8)_2\text{Cl}_2]$  ( $S = 0, 1$  or  $2$ ) and the cation  $[\text{Fe}(\text{L}^8)_2\text{Cl}_2]^+$  ( $S = 1/2, 3/2$  or  $5/2$ ) were optimized to determine the ground state of the  $\text{Fe}(\text{II})$  complexes of this study. Natural bonding orbital (NBO) calculations [32–35] were performed on the optimised structure of ligand  $\text{L}^8$  via the NBO 3.1 module [36] in Gaussian 09, at the same level of theory.

## 3. Results and discussion

The (1,2,3-triazol-4-yl)pyridine ligands ( $\text{L}^2 - \text{L}^9$ ) chosen for this study, contain both electron donating ( $R = \text{CH}_3, \text{OCH}_3$ ) as well as electron withdrawing groups ( $R = \text{F}, \text{Cl}, \text{CN}, \text{CF}_3, \text{COOH}$ ).

### 3.1. Properties of (1,2,3-triazol-4-yl)pyridine free ligands $L^2 - L^9$

The synthesis of the (1,2,3-triazol-4-yl)pyridine free ligands ( $L^2 - L^9$ ) were undertaken, using the copper(I)-catalysed azide alkyne cycloaddition (CuAAC) “click” reaction [1,2], which involves the generation of a five membered triazole ring between an aryl azide and an aryl alkene as shown in Scheme 1.

The  $^1\text{H}$ - and  $^{13}\text{C}$  NMR spectra for each ligand  $L^2 - L^9$  were assigned in comparison with spectra of previously reported triazoles [9,37], and supported by 2-dimensional spectra ( $^1\text{H}$ - $^1\text{H}$  COSY and  $^{13}\text{C}$ - $^1\text{H}$  HMQC), to confirm the proposed assignments. The chemical shift ( $\delta$ ) of the  $^1\text{H}$ -C-H and  $^{13}\text{C}$  NMR (=CH) of the triazole moiety have been tabulated in Table S1, for ligands  $L^2$  to  $L^9$ . The effect of the electron withdrawing substituents on the phenyl ring, manifested itself in shifts of the C-H-triazole peak of the  $^1\text{H}$ -1,2,3-triazole system, which was observed in the range between 8.54 and 9.46 ppm in the  $^1\text{H}$  NMR spectra, and between 119.69 and 120.48 ppm in the  $^{13}\text{C}$  NMR spectra of ligands  $L^2$  to  $L^9$ . The good communication between the different substituents R on the phenyl group and the rest of the ligand, results in a linear trend between the shift of the  $\delta(\text{C-H})$  triazole peak of the  $^1\text{H}$ -1,2,3-triazole system and the para Hammett constant of the R group, see Fig. 2.

The calculated density functional theory (DFT) optimised geometries of ligands  $L^2$  to  $L^9$ , showed that the lowest energy geometry of each ligand has the NH of the triazol ring *syn* to the pyridine nitrogen, in agreement with experimental crystal structures of (1,2,3-triazol-4-yl)pyridine ligands [38]. This preferred orientation can be explained by the stabilisation interaction between the lone pair on  $\text{N}_{\text{triazole}}$ , LP(N), and the antibonding orbital of (C-H)<sub>pyridine</sub>,  $\text{BD}^*(\text{C-H})$ . For ligand 8 (with R = H on  $L^8$ ), for example, the lone pair LP(N) with natural bond orbital (NBO) occupation of 1.928  $e^-$ , donate electron density to the empty antibonding orbital  $\text{BD}^*(\text{C-H})$ , with NBO occupation 0.014  $e^-$ . The NBO calculation of ligand 7 detected this interaction with a second order perturbation energy of 0.5  $\text{kJ}\cdot\text{mol}^{-1}$ ; see Fig. 3 for a visualisation of this interaction.

Although all crystal structures of (1,2,3-triazol-4-yl)pyridine ligands have the NH of the triazol ring in a *syn* position to the pyridine nitrogen, coordination to a metal instead occurs with the nitrogen from the pyridyl and nitrogen group of the 1,2,3-triazole unit (see next unit), unless the  $\text{N}_{\text{triazole}}$  is blocked, for example by having a  $\text{CH}_3$  group attached to it (example CSD reference codes DUSLIO, JOCFAK, JOCFIS, ZOLPUN, WATWOF). This implies that the pyridine group needs to rotate before coordination to a metal can occur. DFT calculations show

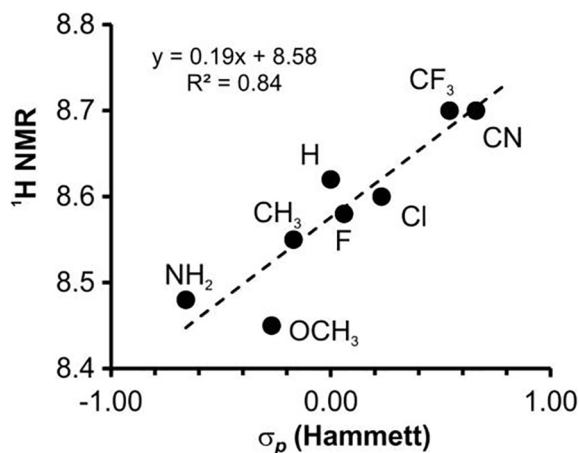


Fig. 2. Relationship between the  $\delta(\text{C-H})$  triazole peak of the  $^1\text{H}$ -1,2,3-triazole system and the para Hammett constant of the R group of the 2-pyridyl-1,2,3-triazole ligands  $L^2 - L^9$ . R group is shown on the graph. Data is given in Table S1. Data (not shown) of ligand with substituent R = COOH ( $L^4$ ) did not fit the trend.

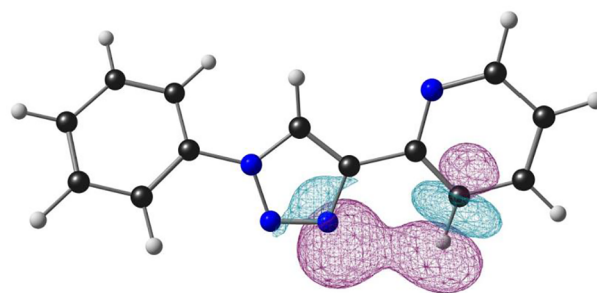


Fig. 3. Optimised geometry of ligand 8 (with group R = H on  $L^8$ ), showing the LP(N)  $\rightarrow$   $\text{BD}^*(\text{C-H})$  NBO interaction. Colour code of atoms (online version): N (blue), O (red), Cl (green), C (black), H (white). (For interpretation of the references to colour in this figure legend, the reader is referred to the web version of this article.)

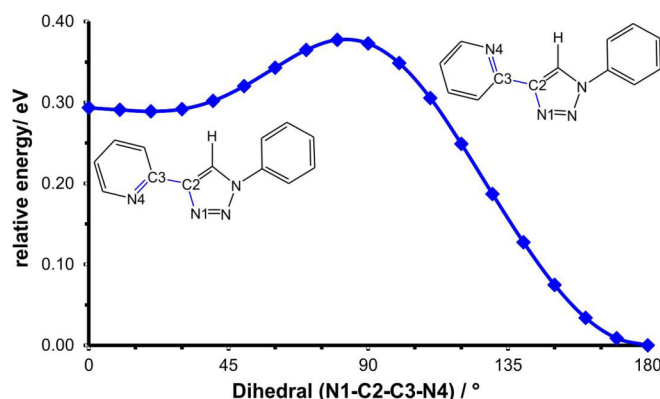


Fig. 4. Potential energy surface scan along the  $\text{N1}_{\text{triazole}}\text{-C2-C3-N4}_{\text{pyridine}}$  dihedral angle of ligand 8 (with group R = H on  $L^8$ ).

that the energy barrier, upon rotation from the optimised *syn* to the optimised *anti* geometry of ligand 8 (with R = H on  $L^8$ ), is only 0.38 eV (36  $\text{kJ}\cdot\text{mol}^{-1}$  or 8.7  $\text{kcal}\cdot\text{mol}^{-1}$ ), which is *ca.* three times the C-C bond rotation barrier of ethane [39], see Fig. 4.

The highest occupied molecular orbitals (HOMOs) of the ligands show extended  $\pi$ -character, which expands over the whole ligand (Fig. 5), explaining the sensitivity of the  $^1\text{H}$  NMR C-H-triazole peak on the electron donating/withdrawing power of the various R substituents on the 2-[1-(4-R-phenyl)-1H-1,2,3-triazol-4-yl]pyridine ligands.

### 3.2. Characterisation of the Fe-ligand complexes

Complex formation of the bidentate (1,2,3-triazol-4-yl)pyridine ligands with iron occur with the pyridyl 1,2,3-triazole nitrogens (Scheme 2). The complexes were prepared in a 1:2 mol ratio of iron : ligand and were characterized by different techniques, such as FT-IR, MS, NMR, UV-Vis, melting points, electrochemistry and computational chemistry calculations. The IR spectra of the Fe compounds exhibited bands with appropriate shifts, due to complex formation. This indicates coordination of the nitrogen from the C=N pyridine moiety, to the iron atom. The coordination mode is determined by the X-ray molecular structure analysis of a crystal of complex 3  $[\text{Fe}(\text{L}^3)_2\text{Cl}_2]$ , with substituent R =  $\text{OCH}_3$  on  $L^3$ , as a representative example of complexes 2 to 9. The experimentally measured magnetic moments for complexes 2–9 are 5.26, 5.07, 5.1, 4.87, 5.10, 4.26, 4.66, 4.72 B.M. respectively, consistent with high spin  $S = 2$  iron(II) complexes. Some iron(II) compounds containing 2-pyridyl-1,2,3-triazole ligands are reported to be low spin [40] and other high spin at room temperature, and some exhibit spin crossover properties [41]. For example, certain iron(II) complexes with ferrocene-containing triazole-pyridine ligands, *trans*- $[\text{Fe}(\text{Fc}t\text{zpy})_2(\text{NCX})_2]\cdot\text{CHCl}_3$  (Fc-tzpy = 4-(2-pyridyl)-1H-1,2,3-triazol-1-

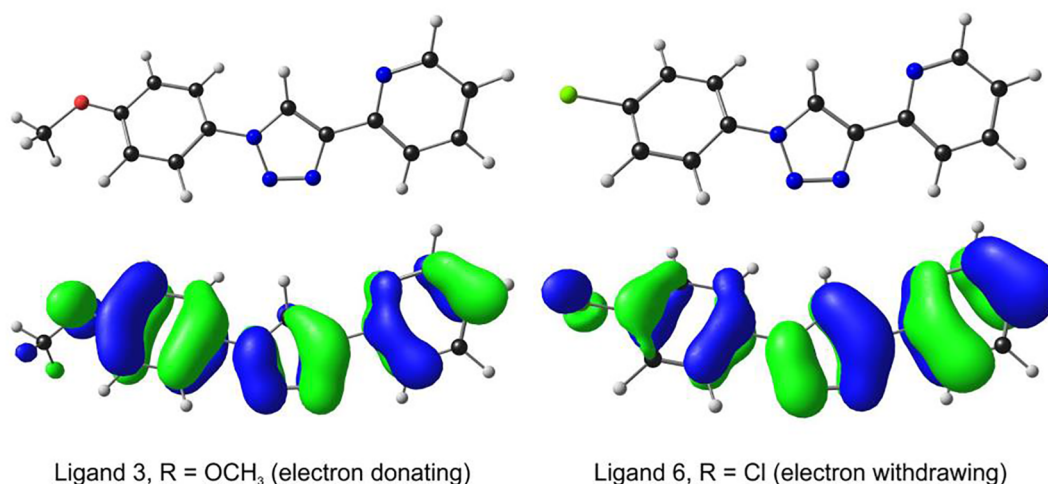


**Fig. 5.** HOMOs of the indicated ligands (with group R = OCH<sub>3</sub> on L<sup>3</sup>; group R = Cl on L<sup>6</sup>). Colour code of atoms (online version): N (blue), O (red), Cl (green), C (black), H (white). A contour value of 30 e/nm<sup>3</sup> has been used to generate the orbital plots. (For interpretation of the references to colour in this figure legend, the reader is referred to the web version of this article.)

ylferrocene, X = S (1') and X = Se (2')) exhibit spin crossover display thermal- and light-induced spin crossover properties. The crystal structure of both 1' (X = S) and 2' (X = Se) at 275 K is consistent with the iron(II) ion in the high-spin state while the crystal structure of 2' (X = Se) at the low temperature of 120 K is consistent with the iron(II) ion in the low-spin state [42].

### 3.2.1. X-ray structure of complex **3** [Fe(L<sup>3</sup>)<sub>2</sub>Cl<sub>2</sub>] with substituent R = OCH<sub>3</sub> on L<sup>3</sup>

A perspective drawing of the molecular structure of complex [Fe(L<sup>3</sup>)<sub>2</sub>Cl<sub>2</sub>] (with substituent R = OCH<sub>3</sub> on L<sup>3</sup>), including the atom numbering scheme, is shown in Fig. 6. Crystallographic data is presented in Table 1, with selected bond lengths (Å) and bond angles (°) listed in Table 2. Complex **3**, [Fe(L<sup>3</sup>)<sub>2</sub>Cl<sub>2</sub>], crystallises in the monoclinic *P2<sub>1</sub>/c* space group. The iron centre in [Fe(L<sup>3</sup>)<sub>2</sub>Cl<sub>2</sub>] is in a distorted octahedral coordination arrangement, which includes two of the 2-(1-

(4-methoxy-phenyl)-1*H*-1,2,3-triazol-4-yl) pyridine ligands, coordinated via the N8<sub>triazol</sub> and N1<sub>pyridine</sub> atoms from the two ligands L<sup>3</sup>, to the iron centre. The iron atom lies on an inversion centre with the asymmetric unit containing the iron, a chloride and one ligand and so the iron coordination requirement is completed by this symmetry operation. The Ni–N1<sub>pyridine</sub>, Ni–N8<sub>triazol</sub> and Ni–Cl bond lengths are 2.2018(15) Å, 2.1838(16) Å and 2.4456(5) Å respectively. The iron-triazole bond length is ca. 0.02 Å shorter than the iron-pyridine bond length. Atoms N8<sup>eq</sup>–Fe–N1<sup>eq</sup> (N<sub>(pyridine)</sub> 1–Fe–N<sub>(triazole)</sub>) lie in the equatorial plane, at an angle of 75.90(6)°. The inversion symmetry means that the N1<sub>pyridine</sub>, N8<sub>triazol</sub> and Cl1 are trans to their symmetry equivalents with bond angles e.g. N8<sup>eq</sup>–Fe–N8i<sup>eq</sup> of 180.0°. The N8–N9, N9–N10 and N8–C7 bond lengths of the 1,2,3-triazole ring are 1.311(2) Å, 1.354(2) Å and 1.360(2) Å respectively, and are essentially the same as the corresponding bond lengths in the free ligand (L<sup>3</sup>), of N8–N9 1.307(4) Å, N9–N10 1.366(6) Å and N8–C7 1.362(5) Å [10].

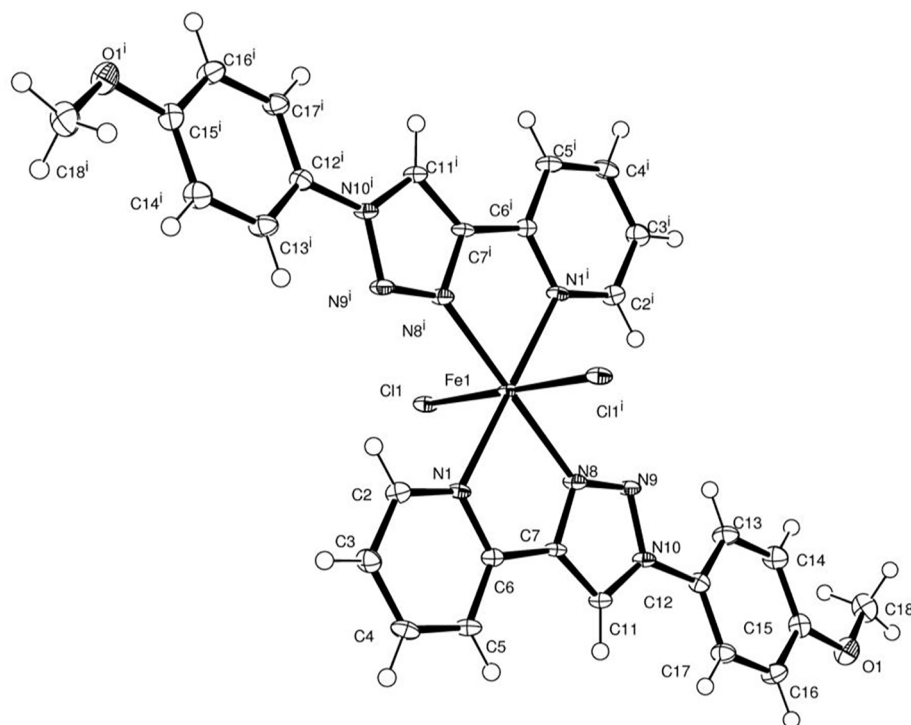


**Fig. 6.** A perspective drawing of the molecular structure of complex [Fe(L<sup>3</sup>)<sub>2</sub>Cl<sub>2</sub>] (with group R = OCH<sub>3</sub> on ligand L<sup>3</sup>), showing the atom numbering scheme. The asymmetric unit contains one half of the complex, with the Fe site lying on an inversion centre, with the other ligand and Cl atom being generated by inversion symmetry. Displacement ellipsoids are drawn at 50% probability level.

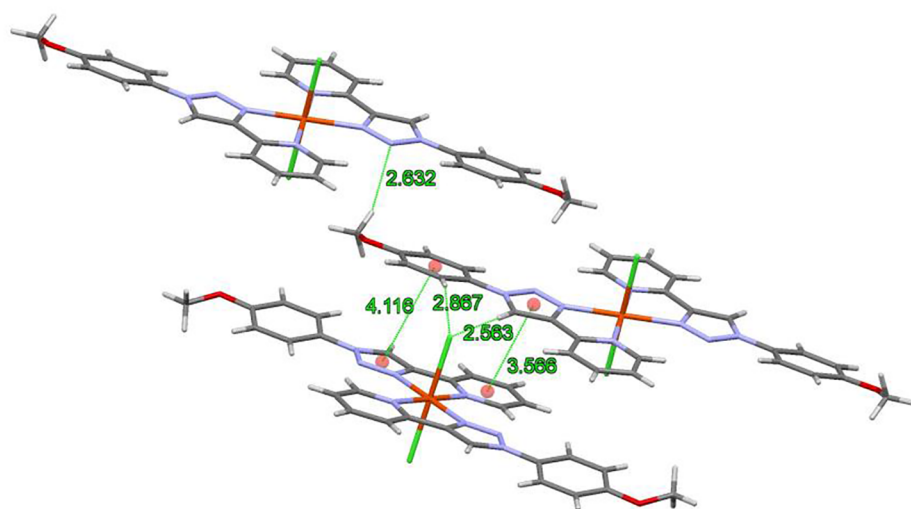


**Fig. 7.** Partial packing of  $[\text{Fe}(\text{L}^3)_2\text{Cl}_2]$ , showing intermolecular hydrogen bonding interactions ( $\text{C}-\text{H}\cdots\text{Cl}$  and  $\text{C}-\text{H}\cdots\text{N}$ ) and  $\pi\cdots\pi$  stacking distances ( $\text{\AA}$ ), involving the triazole – pyridyl and phenyl – triazole rings.

The pyridine ring and the plane through the triazole ring are coplanar with an angle between them of  $0.66^\circ$ , while the plane through the substituted phenyl ring has an angle of  $12.04^\circ$  with the latter. A *trans* orientation of the triazole ligands in the same plane, with the  $\text{N}_{\text{pyridine}}$  and  $\text{N}_{\text{triazole}}$  donors *trans* to each other, has recently been found for octahedral  $[\text{Ni}(\text{L}^2)_2\text{Cl}_2]$  [20],  $[\text{Zn}(\text{L}^2)_2\text{Cl}_2]$  [20],  $[\text{Co}(\text{L}^3)_2\text{Cl}_2]$  [43],  $[\text{Ni}(\text{L}^3)_2\text{Cl}_2]$  [43] and in a related octahedral nickel complex containing two 1-(cyclohexyl)-4-(2-pyridyl)-1,2,3-triazole ligands and two *trans* bromo atoms [44]. A further example is the square planar Pd(II) complex with two 4-(2-Pyridyl)-1-phenyl-1H-1,2,3-triazole ligands [45]. However, in octahedral  $[\text{Mn}(\text{L}^3)_2\text{Cl}_2]$  [43], the two chloro ligands are adopting the *cis* positions around the Mn centre.

Several weak intermolecular hydrogen bonding and  $\pi\cdots\pi$  interactions lead to a 3D supramolecular structure, see Fig. 7. Weak intramolecular hydrogen bonding interactions,  $\text{C}11-\text{H}11\cdots\text{Cl}$  and  $\text{C}17-\text{H}17\cdots\text{Cl}$  involving the chloro moieties, as well as  $\text{C}18-\text{H}18\cdots\text{N}9$  involving the methoxy group, are present with  $\text{H}\cdots\text{Acceptor}$  distances for  $\text{H}11\cdots\text{Cl}$  (2.563  $\text{\AA}$ ) and  $\text{H}17\cdots\text{Cl}$  (2.867  $\text{\AA}$ ) which are well below the sum of the Van der Waals radii of H and Cl (3  $\text{\AA}$ ) [46]. The intramolecular  $\text{H}18\cdots\text{N}9$  distance of 2.632  $\text{\AA}$  is quite long, but still shorter than the sum of their Van der Waals radii (2.75  $\text{\AA}$ ), and is comparable with other published results [47,48]. The triazole  $\text{C}_7\text{N}_8\text{N}_9\text{N}_{10}\text{C}_{11}$  and pyridine  $\text{N}_1\text{C}_2\text{C}_3\text{C}_4\text{C}_5\text{C}_6$  rings stack in a face-to-face parallel manner, exhibiting a centroid-centroid distance of 3.566  $\text{\AA}$  and plane to centroid distance of 3.404  $\text{\AA}$ . The phenyl  $\text{C}_{12}\text{C}_{13}\text{C}_{14}\text{C}_{15}\text{C}_{16}\text{C}_{17}$  and triazole  $\text{C}_7\text{N}_8\text{N}_9\text{N}_{10}\text{C}_{11}$  rings of the neighboring molecules are separated by 4.116  $\text{\AA}$ , with a 3.487  $\text{\AA}$  plane to centroid distance, which is indicative of a slipped-type parallel alignment, see Fig. 7. These distances are comparable to previously reported bond separations typical of  $\pi\cdots\pi$  stacking [49] triazole rings.

### 3.2.2. DFT study of the Fe-complexes

Five geometrical isomers, three *cis* and two *trans*, are possible for each of the eight Fe complexes of this study, containing two (1,2,3-triazol-4-yl)pyridine ligands and two chloride atoms attached to the iron centre. The five isomers for complex  $[\text{Fe}(\text{L}^8)_2\text{Cl}_2]$ , with R = H on ligand  $\text{L}^8$ , are shown in Fig. 8. The  $d^6$   $[\text{Fe}(\text{L})_2\text{Cl}_2]$  complexes of this study are high spin complexes with a  $t_{2g}^4e_g^2$  ground state [50]. This is confirmed by the experimentally measured magnetic moment of 5.07B.M for complex 3. To confirm the spin state of  $S = 2$ , the five isomers of  $[\text{Fe}(\text{L}^8)_2\text{Cl}_2]$  were each optimized for all the possible spin states of a  $d^6$  complex (namely  $S = 0, 1$  or  $2$ ). The relative energies given in Table 3 clearly show, in agreement with experiment, that  $[\text{Fe}(\text{L}^8)_2\text{Cl}_2]$  is high spin with  $S = 2$ . The two lowest energy isomers, one *cis* and one *trans*, are the isomers with the pyridine groups positioned *trans*

to each other. The lowest energy isomer is the same *trans* isomer as has been obtained experimentally for complex  $[\text{Fe}(\text{L}^3)_2\text{Cl}_2]$ , with R =  $\text{OCH}_3$  on ligand  $\text{L}^3$ .

Complexes 2 to 9 of this study are  $d^6$  Fe(II) complexes, with the ligands arranged in a distorted octahedron geometry around Fe(II). Evaluation of the frontier orbitals of the DFT optimised complex 8, shows that the HOMO is 98%  $d_{xy}$  Fe based, see Fig. 9 top. The first electron to be removed upon oxidation of the Fe(II) complex, will thus be a Fe  $d_{xy}$  electron from the HOMO, with the formation of Fe(III). The character of the LUMO of oxidized 8 (93%  $d_{xy}$  Fe), the orbital from which the electron was removed upon oxidation (Fig. 10 bottom), confirms that oxidation of 8 is iron metal based. The HOMO of oxidized 8 (Fig. 10 top), however, has 58% chloride character, suggesting that the next oxidation (experimentally observed at c.a. 0.7 V versus  $\text{Fc}/\text{Fc}^+$ ) involves chloride. The LUMO of the neutral complex 8 is (1,2,3-triazol-4-yl)pyridine ligand based. Reduction of 8 is therefore also (1,2,3-triazol-4-yl)pyridine ligand based. It is not expected that electron withdrawing or donating R substituents will have a large influence on the value of the  $\text{Fe}^{\text{II/III}}$  redox couple, since the HOMO does not have any ligand character whatsoever, that could transpose any electron density via conjugation from the R substituent to Fe.

### 3.2.3. Electrochemistry of the eight Fe-complexes

The cyclic voltammograms of the eight Fe(II) – (1,2,3-triazol-4-yl)pyridine complexes, 2–9, all show the following electrochemical peaks: a small chemical reversible redox couple at ca.  $-0.3$  V versus  $\text{Fc}/\text{Fc}^+$ , two or more irreversible reduction peaks below  $-1.5$  V versus  $\text{Fc}/\text{Fc}^+$ , and an irreversible oxidation peak at ca. 0.7 V versus  $\text{Fc}/\text{Fc}^+$ , see Fig. 11 (left). The chemical reversible redox couple at ca.  $-0.3$  V versus  $\text{Fc}/\text{Fc}^+$  is assigned to the  $\text{Fe}^{\text{II/III}}$  redox couple, based on the character of the HOMO of these complexes, as described in the previous section. The large irreversible oxidation peak at ca. 0.7 V versus  $\text{Fc}/\text{Fc}^+$  is assigned to the chloride oxidation, based on the character of the HOMO of the oxidised complexes (cations), as also described in the previous section. A value of c.a. 0.7 V versus  $\text{Fc}/\text{Fc}^+$  for coordinated chloride oxidation, agree quantitatively with chloride oxidation, since the standard oxidation potential  $\text{Cl}^-$  is 1.34 V versus NHE, i.e. (1.34–0.244) V = 1.1 V versus SCE, or (1.1–0.525) V = 0.58 V versus  $\text{Fc}/\text{Fc}^+$ .

The first observed reduction is assigned to the reduction of the (1,2,3-triazol-4-yl)pyridine ligand, based on the character of the LUMO of the neutral complexes. A graph of the cyclic voltammograms (CVs) of the chemical reversible  $\text{Fe}^{\text{II/III}}$  redox couple at ca.  $-0.3$  V versus  $\text{Fc}/\text{Fc}^+$ , is given in Fig. 11 (right). The values of the  $\text{Fe}^{\text{II/III}}$  redox couple are electrochemically irreversible (meaning large oxidation and reduction peak separations) and vary over a very small potential range of ca.

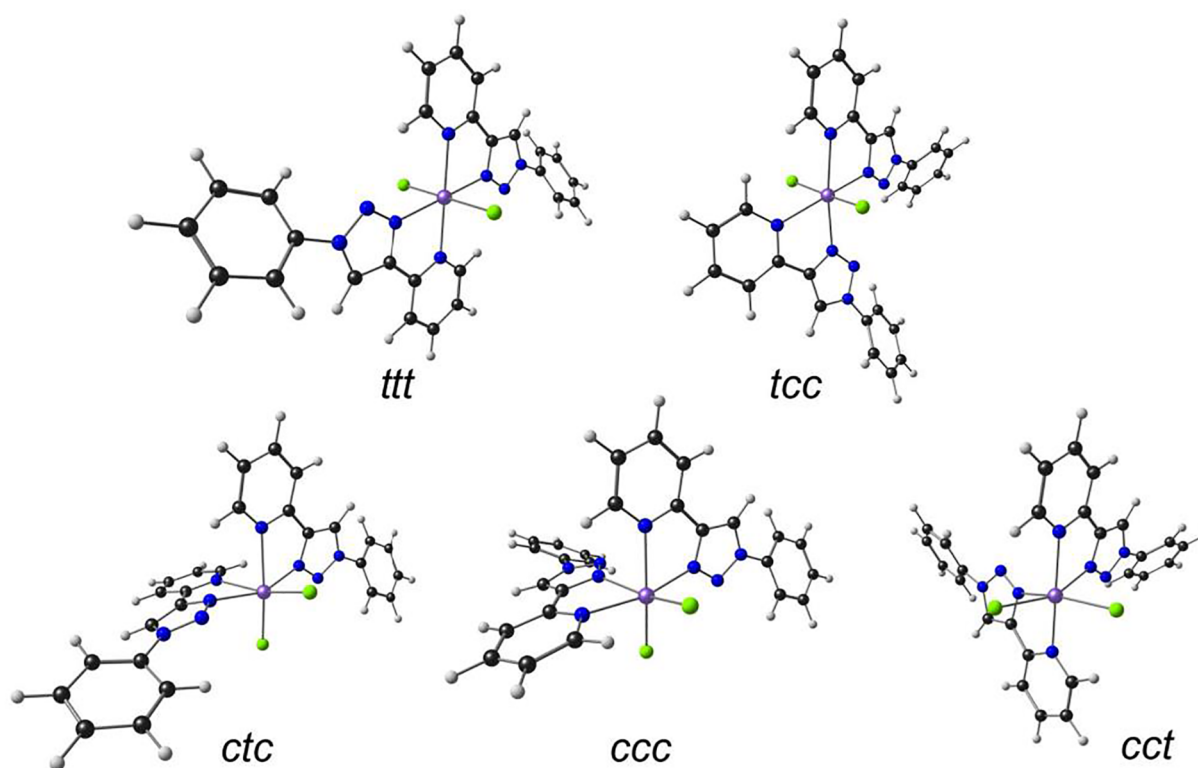


**Fig. 8.** DFT optimized geometries for the two *trans* and three *cis* geometrical isomers possible for complex  $[\text{Fe}(\text{L}^8)_2\text{Cl}_2]$  (with  $\text{R} = \text{H}$  on ligand  $\text{L}^8$ ). The *trans* (*t*) and *cis* (*c*) assignment is according to the relative positions of (1) Cl, (2)  $\text{N}_{\text{triazole}}$  and (3)  $\text{N}_{\text{pyridine}}$ . Colour code of atoms (online version): Fe (purple), Cl (green), N (blue), C (black), H (white). (For interpretation of the references to colour in this figure legend, the reader is referred to the web version of this article.)

**Table 3**

Relative energies (eV) for the different spin states and geometrical isomers of  $[\text{Fe}(\text{L}^8)_2\text{Cl}_2]$ .

Isomer <sup>a</sup>	S	Electronic energy E (eV) <sup>b</sup>	Gibbs energy G (eV)
<i>ctc</i>	0	1.11	1.35
<i>ccc</i>		0.88	1.12
<i>cct</i>		0.63	0.88
<i>ttt</i>		0.61	0.83
<i>tcc</i>		0.89	1.12
<i>ctc</i>	1	1.18	1.26
<i>ccc</i>		0.97	1.07
<i>cct</i>		0.78	0.88
<i>ttt</i>		1.95	2.09
<i>tcc</i>		0.91	0.98
<i>ctc</i>	2	0.48	0.44
<i>ccc</i>		0.27	0.26
<i>cct</i>		0.10	0.10
<i>ttt</i>		0.00	0.00
<i>tcc</i>		0.19	0.16

<sup>a</sup> See Fig. 8 for the geometry of the different isomers.

<sup>b</sup> E from reference [20].

0.05 V, for the  $\text{Fe}^{\text{II/III}}$  redox couple of all eight complexes, 2–9. The various R substituents (Scheme 2) on the eight different ligands ( $\text{L}^2 - \text{L}^9$ ) of these complexes, therefore have virtually no influence on the values of the  $\text{Fe}^{\text{II/III}}$  redox couple for complexes 2–9, as was expected from the character of the HOMOs of complexes 2–9, which did not demonstrate any communication of electron density between the ligand and the Fe metal. A similar result was obtained for a series of eight *fac*- $\text{Re}(\text{CO})_3\text{Cl}$ -pyridyl-1,2,3-triazole containing substituted 2-(1-R-1H-1,2,3-triazol-4-yl)pyridine ligands where the position of the Re-based oxidation were found to be essentially unaffected by the electronic nature of the different R substituents (octyl, Bn, 4-methoxybenzyl, 4-

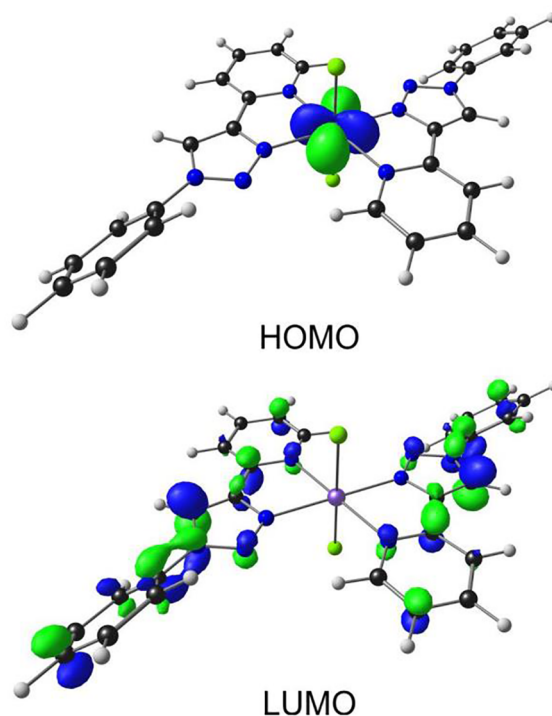


**Fig. 9.** Frontier orbitals of complex  $[\text{Fe}(\text{L}^8)_2\text{Cl}_2]$  (with  $\text{R} = \text{H}$  on ligand  $\text{L}^8$ ). Colour code of atoms (online version): Fe (purple), N (blue), C (black), H (white). A contour value of  $60 \text{ e}/\text{nm}^3$  has been used to generate the orbital plots. Colour code (online version): Fe (purple), C (grey), N (blue) and H (white). (For interpretation of the references to colour in this figure legend, the reader is referred to the web version of this article.)



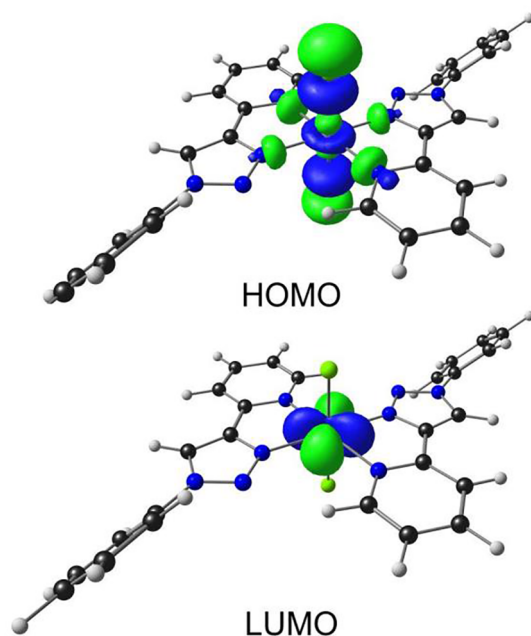


**Fig. 10.** LUMO and HOMO of  $[\text{Fe}(\text{L}^8)_2\text{Cl}_2]^+$  (with R = H on  $\text{L}^8$ ). A contour value of  $60 \text{ e}/\text{nm}^3$  has been used to generate the orbital plots. Colour code of atoms (online version): Fe (purple), N (blue), C (black), H (white). (For interpretation of the references to colour in this figure legend, the reader is referred to the web version of this article.)

nitrobenzyl, phenyl, ferrocenyl, 4-methoxyphenyl and nitrophenyl) [51].

The commonly used iodide/triiodide ( $\text{I}_3^-/\text{I}^-$ ) redox mediator used in dye-sensitized solar cells, DSSC [52] has an average redox potential of  $-0.34 \pm 0.02 \text{ V}$  vs  $\text{Fc}/\text{Fc}^+$  in acetonitrile [53]. Complexes 2–9 with a similar redox potential may thus qualify as alternative redox mediators. “Ultimately, the election of a determined couple as mediator will

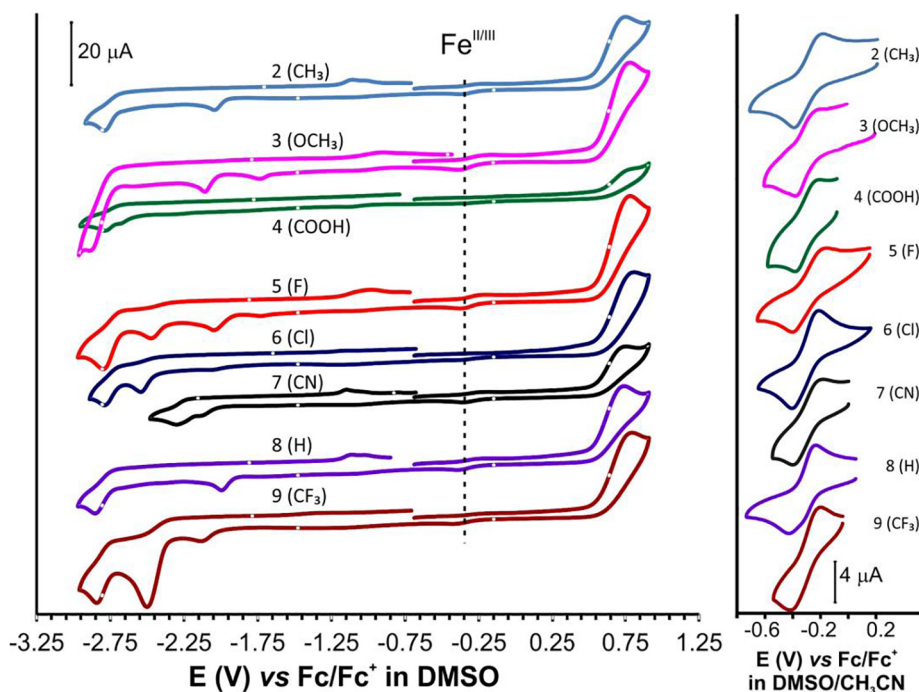


**Fig. 11.** Cyclic voltammograms recorded at  $0.100 \text{ V s}^{-1}$ , of complexes 2 to 9: Left: Wide scans in DMSO, Right: Region of the  $\text{Fe}^{\text{II/III}}$  redox couple for each complex, in DMSO:  $\text{CH}_3\text{CN}$  (1:3) solution. The y-axis denotes relative current. Values  $E^{\text{r}}$  (V vs.  $\text{Fc}/\text{Fc}^+$ ) =  $-0.287$ ,  $-0.282$ ,  $-0.296$ ,  $-0.281$ ,  $-0.311$ ,  $-0.295$ ,  $-0.333$  and  $-0.310 \text{ V}$ , for complexes 2 to 9 respectively.

depend mainly on the electronic properties of the specific dye in a given cell” [54].

#### 4. Summary

Eight different dichloro(bis{2-[1-(4-R-phenyl)-1H-1,2,3-triazol-4-yl- $\kappa\text{N}^3$ ]pyridine- $\kappa\text{N}$ })iron(II) complexes (2–9), with substituents R =  $\text{CH}_3$  ( $\text{L}^2$ ),  $\text{OCH}_3$  ( $\text{L}^3$ ),  $\text{COOH}$  ( $\text{L}^4$ ), F ( $\text{L}^5$ ), Cl ( $\text{L}^6$ ), CN ( $\text{L}^7$ ), H ( $\text{L}^8$ ) and  $\text{CF}_3$  ( $\text{L}^9$ ), have been synthesised and characterised. The single crystal structure of 3 and theoretical DFT calculations both demonstrated a distorted octahedral geometry, with the two triazole ligands coordinated to the iron centre positioned in the equatorial plane, and the two chloro atoms in the axial positions *trans* to each other. The DFT calculations further demonstrated that the  $d^6$   $[\text{Fe}(\text{L})_2\text{Cl}_2]$  complexes of this study is high spin complexes with a  $t_{2g}^4 e_g^2$  ground state. The HOMO of the  $d^6$  Fe(II) complexes is Fe metal-based. The LUMO on the other hand, is (1,2,3-triazol-4-yl)pyridine ligand-based. The cyclic voltammograms of all eight Fe(II) metal (1,2,3-triazol-4-yl)pyridine complexes (2–9), all show a small chemical reversible redox couple at *ca.*  $-0.3 \text{ V}$  versus  $\text{Fc}/\text{Fc}^+$ , which was assigned to the  $\text{Fe}^{\text{II/III}}$  redox couple, based on the character of the HOMO of the Fe-complexes. A second irreversible oxidation peak at *ca.*  $0.7 \text{ V}$  versus  $\text{Fc}/\text{Fc}^+$  was assigned to the chloride oxidation, while the first observed reduction (below  $-1.5 \text{ V}$ ) was assigned to the reduction of the (1,2,3-triazol-4-yl)pyridine ligand, based on the character of the LUMO of the neutral complexes. The different R substituents on the phenyl rings of complexes 2–9 did not in any way influence the values of the metal  $\text{Fe}^{\text{II/III}}$  redox couple, which only varied over a small potential range of only  $0.05 \text{ V}$ . This ligand independency can be explained by the character of the HOMOs of complexes 2–9, which did not demonstrate any communication of electron density between the ligands and the Fe metal. The HOMOs of the free ligands, however, displayed extended  $\pi$ -character which expands over the entire ligand, explaining the sensitivity of the  $^1\text{H}$  NMR C–H-triazole peak, which is dependent on the electron donating/withdrawing power of the different R substituents on the eight 2-[1-(4-R-phenyl)-1H-1,2,3-triazol-4-yl]pyridine ligands.

## Acknowledgements

The National Mass Spectroscopy Centre at the University of Wales, Swansea is thanked for supplying the mass spectrometry data. XRD data and structures were supplied by the National Crystallography Service at the University of Southampton. KT expresses his gratitude to the Iraqi Government for financial support to conduct the research reported in the UK and EPSRC for funding the UK National Crystallography Service. This work has received support from the South African National Research Foundation and the Central Research Fund of the University of the Free State, Bloemfontein, South Africa. The authors acknowledge the High Performance Computing facility of the University of the Free State and the Centre for High Performance Computing (CHPC), South Africa, for providing computational resources to this research project.

## Appendix A. Supplementary data

Supplementary data (Optimised coordinates of the DFT calculations and crystallographic data for **3**) are given in the Supporting Information at <https://doi.org/10.1016/j.ica.2018.09.056>.

## References

- M.B. Smith, J. March, March's advanced organic chemistry: reactions mechanisms, and structure, *Molecules* 6 (2001) 1064–1065, <https://doi.org/10.3390/61201064>.
- M.B. Smith, *Organic Synthesis Second Edition*, 3.9. A Oxidation of Sulfur Compounds, Department of Chemistry, University of Connecticut, USA, 2002.
- E.J. Corey, Enantioselective catalysis based on cationic oxazaborolidines, *Angew. Chem. Int. Ed.* 48 (2009) 2100–2117, <https://doi.org/10.1002/anie.200805374>.
- J.D. Worley, *Heterocyclic chemistry*, second edition (Gilchrist, T.L.), *J. Chem. Educ.* 70 (1993) A89, <https://doi.org/10.1021/ed070pA89.1>.
- B. Schulzeab, U.S. Schubert, Beyond click chemistry – supramolecular interactions of 1,2,3-triazoles, *Chem. Soc. Rev.* 43 (2014) 2522–2571, <https://doi.org/10.1039/c3cs60386e>.
- R.N. Kumar, G. Mallareddy, P. Nagender, P.S. Rao, Y. Poornachandra, P. Ranjithreddy, C.G. Kumar, B. Narsaiah, Synthesis of novel triazole functionalized pyridine derivatives as potential antimicrobial and anti-biofilm agents, *IJC*, 55B (11) 1361–1375. < <http://nopr.niscair.res.in/handle/123456789/37033> > .
- H.Y.V. Ching, X. Wang, M. He, N.P. Holland, R. Guillot, C. Slim, S. Griveau, H.C. Bertrand, C. Pollicar, F. Bedoui, M. Fontecave, Rhenium complexes based on 2-pyridyl-1,2,3-triazole ligands: a new class of CO<sub>2</sub> reduction catalysts, *Inorg. Chem.* 56 (2017) 2966–2976, <https://doi.org/10.1021/acs.inorgchem.6b03078>.
- L. Liang, D. Astruc, The copper(I)-catalyzed alkyne-azide cycloaddition (CuAAC) “click” reaction and its applications. an overview, *Coord. Chem. Rev.* 255 (2011) 2933–2945, <https://doi.org/10.1016/j.ccr.2011.06.028>.
- S. Paek, C. Baik, M. Kang, H. Kang, J. Ko, New type of ruthenium sensitizers with a triazole moiety as a bridging group, *J. Organometal. Chem.* 695 (2010) 821–826, <https://doi.org/10.1016/j.jorganchem.2009.12.021>.
- K.M. Tawfiq, G.J. Miller, M.J. Al-Jeboori, P.S. Fennell, S.J. Coles, G.J. Tizzard, C. Wilson, H. Potgieter, Comparison of the structural motifs and packing arrangements of six novel derivatives and one polymorph of 2-(1-phenyl-1H-1,2,3-triazol-4-yl)pyridine, *Acta Cryst. B* 70 (2014) 379–389, <https://doi.org/10.1107/S2052520614001152>.
- D. Kumar, V.B. Reddy, An efficient, one-pot, regioselective synthesis of 1,4-diaryl-1H-1,2,3-triazoles using click chemistry, *Synthesis* (2010) 1687–1691, <https://doi.org/10.1055/s-0029-1218765>.
- F. Alonso, Y. Moglie, G. Radivov, M. Yus, Click chemistry from organic halides, diazonium salts and anilines in water catalysed by copper nanoparticles on activated carbon, *Org. Biomol. Chem.* 9 (2011) 6385–6395, <https://doi.org/10.1039/C1OB05735A>.
- I.S. Park, M.S. Kwon, Y. Kim, J.S. Lee, J. Park, Heterogeneous copper catalyst for the cycloaddition of azides and alkynes without additives under ambient conditions, *Org. Lett.* 10 (2008) 497–500, <https://doi.org/10.1021/ol702790w>.
- H. Park, *Pharmaceutical Patent Analyst*, 3 (2014) 491–498.
- M. Wolff, L. Munoz, A. François, C. Carrayon, A. Seridi, N. Saffon, C. Picard, B. Machura, E. Benoist, Tricarbonylrhenium complexes from 2-pyridyl-1,2,3-triazole ligands bearing a 4-substituted phenyl arm: a combined experimental and theoretical study, *J. Chem. Soc. Dalton Trans.* 42 (2013) 7019–7031, <https://doi.org/10.1039/C3DT33071K>.
- D. Schweinfurth, R. Pattacini, S. Strobel, B. Sarkar, New 1,2,3-triazole ligands through click reactions and their palladium and platinum complexes, *J. Chem. Soc. Dalton Trans.* (2009) 9291–9297, <https://doi.org/10.1039/B910660J>.
- J.D. Crowley, P.H. Banteen, L.R. Hanton, A one pot multi-component CuAAC “click” approach to bidentate and tridentate pyridyl-1,2,3-triazole ligands: Synthesis, X-ray structures and copper(II) and silver(I) complexes, *Polyhedron* 29 (2010) 70–83, <https://doi.org/10.1016/j.poly.2009.06.010>.
- K.J. Kilpin, E.L. Gavey, C.J. McAdam, C.B. Anderson, S.J. Lind, C.C. Keep, K.C. Gordon, J.D. Crowley, Palladium(II) Complexes of readily functionalized bidentate 2-pyridyl-1,2,3-triazole “click” ligands: a synthetic, structural, spectroscopic, and computational study, *Inorg. Chem.* 50 (2011) 6334–6346, <https://doi.org/10.1021/ic200789b>.
- J.P. Byrne, J.A. Kitchen, O. Kotova, V. Leigh, A.P. Bell, J.J. Boland, M. Albrecht, Th. Gunnlaugsson, Synthesis, structural, photophysical and electrochemical studies of various d-metal complexes of btp [2,6-bis(1,2,3-triazol-4-yl)pyridine] ligands that give rise to the formation of metallo-supramolecular gels, *Dalton Trans.* 43 (2014) 196–209, <https://doi.org/10.1039/C3DT52309H>.
- J. Conradie, M.M. Conradie, K.M. Tawfiq, M.J. Al-Jeboori, S.J. Coles, C. Wilson, J.H. Potgieter, Novel dichloro(bis[2-[1-(4-methylphenyl)-1H-1,2,3-triazol-4-yl- $\&$  N<sup>3</sup>]pyridine- $\&$ N])metal(II) coordination compounds of seven transition metals (Mn, Fe Co, Ni, Cu, Zn and Cd), *Polyhedron* 151 (2018) 243–254, <https://doi.org/10.1016/j.poly.2018.03.026>.
- G.A. Bain, J.F. Berry, Diamagnetic corrections and pascal's constants, *J. Chem. Educ.* 85 (2008) 532–536, <https://doi.org/10.1021/ed085p532>.
- S.J. Coles, P.A. Gale, Changing and challenging times for service crystallography, *Chem. Sci.* 3 (2012) 683–689, <https://doi.org/10.1039/C2SC00955B>.
- O.V. Dolomanov, L.J. Bourhis, R.J. Gildea, J.A.K. Howard, H. Puschmann, OLEX2: a complete structure solution, refinement and analysis program, *J. Appl. Cryst.* 42 (2009) 339–341, <https://doi.org/10.1107/S0021889808042726>.
- G.M. Sheldrick, A short history of SHELX, *Acta Cryst. Sect. A* 64 (2008) 112–122, <https://doi.org/10.1107/S0108767307043930>.
- P.T. Kissinger, W.R. Heineman, *Cyclic Voltammetry*, *J. Chem. Ed.* 60 (1983) 702–706, <https://doi.org/10.1021/ed060p702>.
- D.T. Sawyer, J.L. Roberts Jr, *Experimental Electrochemistry for Chemists*, Wiley, New York, 1974, p. 54.
- D.H. Evans, K.M. O'Connell, R.A. Peterson, M.J. Kelly, *Cyclic voltammetry*, *J. Chem. Ed.* 60 (1983) 290–292, <https://doi.org/10.1021/ed060p290>.
- G.A. Mabbott, An introduction to cyclic voltammetry, *J. Chem. Ed.* 60 (1983) 697–702, <https://doi.org/10.1021/ed060p697>.
- G. Gritzner, J. Kuta, Recommendations on reporting electrode potentials in non-aqueous solvents, *Pure Appl. Chem.* 56 (1984) 461–466, <https://doi.org/10.1351/pac198456040461>.
- H.-M. Koepf, H. Wendt, H. Strehlow, Comparison of the potential series in different solvents, *Zeitschrift für Elektrochemie* 64 (1960) 483–491, <https://doi.org/10.1002/bbpc.19600640406>.
- M.J. Frisch, G.W. Trucks, H.B. Schlegel, G.E. Scuseria, M.A. Robb, J.R. Cheeseman, G. Scalmani, V. Barone, B. Mennucci, G.A. Petersson, H. Nakatsuji, M. Caricato, X. Li, H.P. Hratchian, A.F. Izmaylov, J. Bloino, G. Zheng, J.L. Sonnenberg, M. Hada, M. Ehara, K. Toyota, R. Fukuda, J. Hasegawa, M. Ishida, T. Nakajima, Y. Honda, O. Kitao, H. Nakai, T. Vreven, J.A. Montgomery Jr., J.E. Peralta, F. Ogliaro, M. Bearpark, J.J. Heyd, E. Brothers, K.N. Kudin, V.N. Staroverov, R. Kobayashi, J. Normand, K. Raghavachari, A. Rendell, J.C. Burant, S.S. Iyengar, J. Tomasi, M. Cossi, N. Rega, J.M. Millam, M. Klene, J.E. Knox, J.B. Cross, V. Bakken, C. Adamo, J. Jaramillo, R. Gomperts, R.E. Stratmann, O. Yazyev, A.J. Austin, R. Cammi, C. Pomelli, J.W. Ochterski, R.L. Martin, K. Morokuma, V.G. Zakrzewski, G.A. Voth, P. Salvador, J.J. Dannenberg, S. Dapprich, A.D. Daniels, O. Farkas, J.B. Foresman, J.V. Ortiz, J. Cioslowski, D.J. Fox, *Gaussian 09, Revision D.01*, Gaussian, Inc., Wallingford, CT, 2009.
- J.P. Foster, F. Weinhold, Natural hybrid orbitals, *J. Am. Chem. Soc.* 102 (1980) 7211–7218, <https://doi.org/10.1021/ja00544a007>.
- A.E. Reed, F. Weinhold, Natural localized molecular orbitals, *J. Phys. Chem.* 83 (1985) 1736–1740, <https://doi.org/10.1063/1.449360>.
- A.E. Reed, R.B. Weinstock, F. Weinhold, Natural population analysis, *J. Chem. Phys.* 83 (1985) 735–746, <https://doi.org/10.1063/1.449486>.
- A.E. Reed, L.A. Curtiss, F. Weinhold, Intermolecular interactions from a natural bond orbital, donor-acceptor viewpoint, *Chem. Rev.* 88 (1988) 899–926, <https://doi.org/10.1021/cr00088a005>.
- E.D. Glendening, J.K. Badenhop, A.E. Reed, J.E. Carpenter, J.A. Bohmann, C.M. Morales, C.R. Landis, F. Weinhold, NBO 3.1, *Theoretical Chemistry Institute*, University of Wisconsin, Madison, WI, 2001.
- D. Schweinfurth, S. Strobel, B. Sarkar, Expanding the scope of ‘Click’ derived 1,2,3-triazole ligands: New palladium and platinum complexes, *Inorg. Chim. Acta* 374 (2011) 253–260, <https://doi.org/10.1016/j.ica.2011.02.085>.
- Cambridge Structural Database (CSD), Version 5.38, May 2017 update, Cambridge, UK, 2017.
- S. Liu, Origin and nature of bond rotation barriers: a unified view, *J. Phys. Chem. A* 117 (2013) 962–965, <https://doi.org/10.1021/jp312521z>.
- S.K. Vellas, J.E.M. Lewis, M. Shankar, A. Sagatova, J.D.A. Tyndall, B.C. Monk, C.M. Fitchett, L.R. Hanton, J.D. Crowley, [Fe2L3]4+ cylinders derived from Bis(bidentate) 2-pyridyl-1,2,3-triazole “click” ligands: synthesis, structures and exploration of biological activity, *Molecules* 18 (2013) 6383–6407, <https://doi.org/10.3390/molecules18066383>.
- R.W. Hogue, R.G. Miller, N.G. White, H.L.C. Feltham, G.N.L. Jameson, S. Brooker, Hysteretic spin crossover in iron(II) complexes of a new pyridine–triazole–pyrazine ligand is tuned by choice of NCE co-ligand, *Chem. Commun.* 50 (2014) 1435–1437, <https://doi.org/10.1039/C3CC43922D>.
- T. Romero-Morillo, F.J. Valverde-Muñoz, L. Piñeiro-López, M.C. Muñoz, T. Romero, P. Molinac, J.A. Rea, Spin crossover in iron(II) complexes with ferrocene-bearing triazole-pyridine ligands, *Dalton Trans.* 44 (2015) 18911–18918, <https://doi.org/10.1039/c5dt03084f>.
- J. Conradie, M.M. Conradie, K.M. Tawfiq, M.J. Al-Jeboori, S.J. Coles, J.H. Potgieter, Synthesis, characterisation, experimental and electronic structure of novel dichloro(bis[2-[1-(4-methoxyphenyl)-1H-1,2,3-triazol-4-yl-kN3]pyridine-kN])metal(II) compounds, metal = Mn, Co and Ni, *J. Mol. Struct.* 1161C (2018) 89–99, <https://doi.org/10.1016/j.molstruc.2018.02.036>.
- D. Schweinfurth, C.Y. Su, S.C. Wei, P. Braunsteind, B. Sarkar, Nickel complexes with

- “click”-derived pyridyl-triazole ligands: weak intermolecular interactions and catalytic ethylene oligomerisation, *Dalton Trans.* 41 (2012) 12984–12990, <https://doi.org/10.1039/C2DT31805A>.
- [45] (a) A. Dogan, B. Sarkar, A. Klein, F. Lissner, T. Schleid, J. Fiedler, S. Zális, V.K. Jain, W. Kaim, Complex reduction chemistry of (abpy)PtCl<sub>2</sub>, abpy = 2,2'-azobispyridine: formation of cyclic [(micro, eta2:eta1-abpy)PtCl]<sub>2</sub>(2+) with a new coordination mode for abpy and a near-infrared ligand-to-ligand intervalence charge transfer absorption of the one-electron reduced state, *Inorg. Chem.* 43 (2004) 5973–5980, <https://doi.org/10.1021/ic049941t>;  
(b) K.J. Kilpin, J.D. Crowley, Palladium(II) and platinum(II) complexes of bidentate 2-pyridyl-1,2,3-triazole “click” ligands: Synthesis, properties and X-ray structures, *Polyhedron* 29 (2010) 3111–3117, <https://doi.org/10.1016/j.poly.2010.08.021>.
- [46] C.B. Aakeröy, T.A. Evans, K.R. Seddon, I. Pálincó, The C–H–Cl hydrogen bond: does it exist, *New J. Chem.* 23 (1999) 145–152, <https://doi.org/10.1039/A809309A>.
- [47] D. Urankar, A. Pevec, I. Turel, J.G. Košmrlj, Pyridyl conjugated 1,2,3-Triazole is a versatile coordination ability ligand enabling supramolecular associations, *Cryst. Growth Des.* 10 (2010) 4920–4927, <https://doi.org/10.1021/cg100993k>.
- [48] (a) M. Mazik, D. Bläser, R. Boese, The potential of CH–N interactions in determining the crystal structures of novel 3,4-disubstituted-5-pyridinyl-isoxazoles, *Tetrahedron Lett.* 41 (2000) 5827–5831, [https://doi.org/10.1016/S0040-4039\(00\)00906-0](https://doi.org/10.1016/S0040-4039(00)00906-0);  
(b) M. Mazik, D. Bläser, R. Boese, Intermolecular CH…N/CH…O hydrogen bonds in the crystal structures of  $\alpha$ ,  $\beta$ -unsaturated ketones carrying a terminal pyridine subunit, *Tetrahedron* 57 (2001) 5791–5797, [https://doi.org/10.1016/S0040-4020\(01\)00520-8](https://doi.org/10.1016/S0040-4020(01)00520-8).
- [49] (a) Y. Yang, P. Du, J. Yang, W.Q. Kan, J.F. Ma, A series of Cu(II) and Cd(II) coordination polymers constructed by 3,5-dinitrosalicylic acid and flexible bis(triazole) ligands containing different spacers, *Cryst. Eng. Commun.* 15 (2013) 4357–4371, <https://doi.org/10.1039/C3CE00034F>;  
(b) C. Janiak, A critical account on  $\pi$ – $\pi$  stacking in metal complexes with aromatic nitrogen-containing ligands, *J. Chem. Soc. Dalton Trans.* (2000) 3885–3896, <https://doi.org/10.1039/B003010O>.
- [50] G. Sowjanya, N.C.G. Reddy, S.L. Reddy, B.J. Reddy, R.L. Frost, Electron paramagnetic resonance and optical absorption spectral studies on covellite mineral, *Spectrochim. Acta Part A* 71 (2008) 751–754, <https://doi.org/10.1016/j.saa.2007.12.053>.
- [51] T.Y. Kim, A.B.S. Elliott, K.J. Shaffer, C.J. McAdam, K.C. Gordon, J.D. Crowley, Rhenium(I) complexes of readily functionalized bidentate pyridyl-1,2,3-triazole “click” ligands: A systematic synthetic, spectroscopic and computational study, *Polyhedron* 52 (2013) 1391–1398, <https://doi.org/10.1016/j.poly.2012.05.003>.
- [52] G. Boschloo, A. Hagfeldt, Characteristics of the Iodide/Triiodide Redox Mediator in Dye-Sensitized Solar Cells, *Acc. Chem. Res.* 42 (2009) 1819–1826, <https://doi.org/10.1021/ar900138m>.
- [53] X. Wang, D.M. Stanbury, The Oxidation of Iodide by a Series of Fe(III) Complexes in Acetonitrile, *Inorg. Chem.* 45 (2006) 3415–3423, <https://doi.org/10.1021/ic052022y>.
- [54] F. Gajardo, B. Loeb, Spectroscopic and electrochemical properties of a series of substituted polypyridine Co(II)/Co(III) couples and their potentiality as mediators for solar cells, *J. Chilean Chem. Soc.* 56 (2) (2011) 697–701, <https://doi.org/10.4067/S0717-97072011000200016>.